Electronic Supplementary Information (ESI) for:

Engineering high-performance Pd core-MgO porous shell nanocatalysts via heterogeneous gas-phase synthesis

Vidyadhar Singh,[a] Cathal Cassidy,[a] Frank Abild-Pedersen,[b] Jeong-Hwan Kim,[a] Kengo Aranishi,[a] Sushant Kumar,[a] Chhagan Lal,[a] Christian Gspan,[c] Werner Grogger,[c] and Mukhles Sowwan [a,*]

[a]Nanoparticles by Design Unit, Okinawa Institute of Science and Technology (OIST) Graduate University, 1919-1 Onna-Son, Okinawa, 904-0495, Japan.

[b]SUNCAT Center for Interface Science and Catalysis, SLAC National Accelerator Laboratory, 2575 Sand Hill Road, Menlo Park, CA, 94025, USA.

[c]Graz Centre for Electron Microscopy, 8010 Graz, Austria

Table of contents:

Experimental

S1 Materials; **S2** Methods; **S3** Equipment and Techniques

Supplementary Information Figure S1†-S8†:

Fig. S1. Schematic of the magnetron sputter inert gas condensation setup used for the synthesis of core-shell Pd@MgO nanocatlysts.

Fig. S2. GIXRD pattern of of core-shell Pd@MgO nanoparticles on a silicon substrate at a fixed grazing angle of 0.2°.

Fig. S3. TEM images of (a) Pd and (b) MgO nanoparticles, deposited separately. It is evident that the MgO structures have formed porous hollow shells.

Fig. S4. XPS survey spectrum of core-shell Pd@MgO nanoparticles.

Fig. S5. AFM images of Pd@MgO nanoparticles for different Pd/Mg sputtering power ratios; (a) 0.66, (b) 0.33, (c) 0.14, and (d) 0.11.

Fig. S6. I-t curves measured at -0.35 V in 1 M KOH containing 0.5 M MeOH.

Fig. S7. TEM images of (a) coalesced Pd nanoparticles and (b) Pd@MgO core-shell nanoparticles. These samples were used for the catalyst studies

Fig. S8. Pd nanoparticle surface area loss as a result of nanoparticle coalescence on the substrate.

Experimental

S1. Materials

Magnesium magnetron-sputtering target (Mg, purity >99.95%) and Palladium magnetron sputtering target (Pd, purity >99.95%) with dimensions of 25 mm diameter × 3 mm thick were purchased from Kurt J. Lesker (PA, USA). High purity methanol, acetone, isopropanol, were purchased from Sigma-Aldrich Japan. As substrates for AFM and XPS measurements, undoped Si dice with (100) orientation and 5 mm × 5 mm in size were purchased from MTI Corporation (CA, USA). Cu frames with electron transparent carbon coated grids (400 mesh) and silicon nitride membranes were purchased from Ted Pella Inc. (CA, USA), as substrates for TEM/STEM-HAADF analysis.

S2. Methods

Pd, MgO, and Pd@MgO Nanoparticles synthesis:

The *Pd, MgO, and Pd@MgO* nanoparticles were synthesized using magnetron-sputtering with inert-gas aggregation system (Mantis Deposition Ltd, UK), as illustrated in Fig. S1†. The deposition system consists of a nanocluster sputtering source, a quadrupole mass filter (QMF) and a deposition chamber. Mg and Pd sputtering targets were located side-by-side on an integrated magnetron sputtering head, as shown in Fig. S1† (inset). The desired physical and chemical properties of multicomponent hybrid nanoparticles can be tailored by controlling the size of the nanoparticles, as well as the volume fraction of each component. In our experimental configuration this was achieved by tuning the magnetron power applied on each target independently while co-sputtering. Preliminary studies were conducted to identify suitable deposition parameters for both materials, via in situ QMF feedback and deposited cluster characterization. Ar and He flow rates were 90 and 10 sccm (respectively), resulting in an aggregation zone pressure reading of 3.5×10^{-1} mbar. The aggregation zone length was set to 100 mm. The base pressure was 1.0×10^{-8} mbar in the main deposition chamber. For the present study we have used three magnetrons with one palladium and two magnesium targets. A series of samples was produced, keeping the same flow of argon and helium to the magnetrons. The only parameter that was adjusted was the DC power applied to each magnetron. In the sample deposition series, the nanoparticle composition ranged from pure Mg to pure Pd, passing through four intermediate chemical compositions. Tuning of the core-shell nanoparticle size was achieved by varying the sputtering power supplied to the Pd target (7.5 W to 30 W) and Mg target (45 W to 65 W). For comparison, we have deposited Mg and Pd, with the same conditions, separately onto the same substrates, sequentially rather than simultaneously. The nanoparticles were deposited on either (holey) carbon coated Cu/Au grids or on 8 nm thick silicon nitride membranes. In order to obtain suitable substrate coverage, the deposition time ranged from a few minutes (for preliminary TEM structure characterizations on mono-disperse nanoparticles) up to 15 minutes (for electrochemistry studies).

S3. Equipment and Techniques

Characterization techniques:

A Bruker Multimode 8 atomic force microscope (AFM) was used to analyze the topography of the samples. The AFM System, equipped with the NanoScope®V controller, was utilized in tapping mode using a triangular silicon-nitride AFM tip (radius <10 nm, force constant of 0.35 N m^{-1}, 65 kHz of resonant frequency).

HR-TEM studies were carried out using an FEI Titan microscope, operated at both 80kV and 300kV, equipped with a spherical aberration corrector for the image. In image-corrected TEM mode, the spherical and chromatic aberrations were <5 µm and 1.4 mm, respectively, with an optimum resolution of better than 0.09 nm. TEM image simulations were performed using the JEMS software package.[1]

HR-STEM studies were performed on a FEI Titan^3 G2 microscope with a C_S-corrector for the probe. STEM-HAADF and BF images were recorded at 300 kV with a convergence angle of 19.9 mrad and a camera length of 91 mm. EDX measurements were done with a Super-X detector system from Bruker with a step size of 0.06 nm and a pixel time of 0.08 s (number of cycles: 10) for the line scan.

XPS measurements were performed in a Kratos AXIS Ultra DLD Photoelectron spectrometer, with a Mg K_α anode (1253.6 eV), and a base pressure of 2×10^{-9} mbar. The Mg $2p$, Pd $3d$ and O $1s$ core level narrow spectra were recorded using pass energy of 20 eV for high resolution.

Grazing incidence x-ray diffraction (GIXRD) measurements were performed in a Bruker D8 Discover XRD (thin film system), using Cu K_α radiation (40 kV / 40 mA) at a fixed grazing incidence angle of 0.2°.

Electrochemical measurements:

Preparation of nanoparticle catalysts on glassy carbon electrode substrates: Nanoparticles were directly deposited onto the electrode surface inside the Mantis UHV nanoparticle sputtering system. Nanoparticle dimensions and surface coverage were evaluated using TEM images, and associated mass was calculated assuming bulk density values. The estimated loading of catalyst to be 0.085 µg and 0.034 µg for Pd and Pd@MgO samples, respectively.

Electrochemical characterization: The electrocatalysis measurements were performed at room temperature with an electrochemical workstation 440B (CH Instruments Co., US). A conventional three-electrode system was used, which consists of a nanoparticles-modified glassy carbon electrode as the working electrode, a Pt wire as the counter-electrode, and an Ag/AgCl (3 M KCl) electrode as the reference electrode. All working solutions (1 M KOH) were purged with nitrogen for 30 min before measurements.

DFT simulations:

Stepped Pd surfaces in the fcc(211) structure with varying Mg content were used to simulate the chemistry at the core-shell interface. The fcc (211) structure was modeled using 12 atomic layers in a (1 × 3) slab. For each cell more than 13 Å of vacuum in the z-direction separated the slabs. All non-equivalent sites on the different surface orientations were tested but only the most stable binding configurations found are shown in the main text (**Fig. 4)**. All adsorption free energies are calculated relative to H_2O(l), H_2(g), and CO_2(g), where the free energy of H_2O(l) is obtained from H_2O(g) at the equilibrium vapor pressure of 0.035 bar, such that

$$\begin{aligned}\Delta G_{H_xCO_y*} = {} & E^{total}_{H_xCO_y} + (2-y)E^{total}_{H_2O} - E^{total}_{CO_2} - (2+\frac{x}{2}-y)E^{total}_{H_2} - E^{total}_{surf} \\ & + ZPE_{H_xCO_y} + (2-y)ZPE_{H_2O} - ZPE_{CO_2} - (2+\frac{x}{2}-y)ZPE_{H_2} \\ & + C_p dT_{H_xCO_y} + (2-y)C_p dT_{H_2O} - C_p dT_{CO_2} - (2+\frac{x}{2}-y)C_p dT_{H_2} \\ & - T(S_{H_xCO_y} + (2-y)S_{H_2O} - S_{CO_2} - (2+\frac{x}{2}-y)S_{H_2})\end{aligned}$$

Applying the reversible hydrogen electrode as our reference, the effect of the potential *U* is accounted for by shifting the energy of the electrons by -*eU*, where *e* is the elementary charge. If we assume that all proton transfer barriers in the oxidation process are negligible then the over potential and its variation among the different surfaces can to first approximation be estimated as the energy difference between the highest elementary steps in the process.

Supplementary Information Figure S1-S8†:

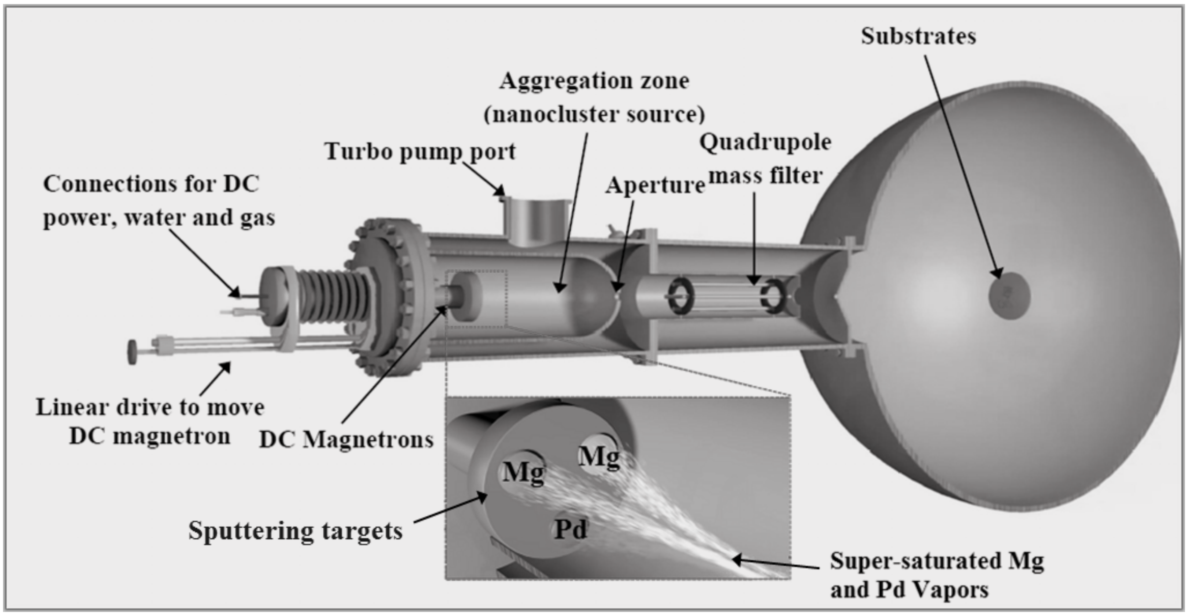

Fig. S1 Schematic of the magnetron sputter inert gas condensation setup used for the synthesis of core-shell Pd@MgO nanocatlysts.

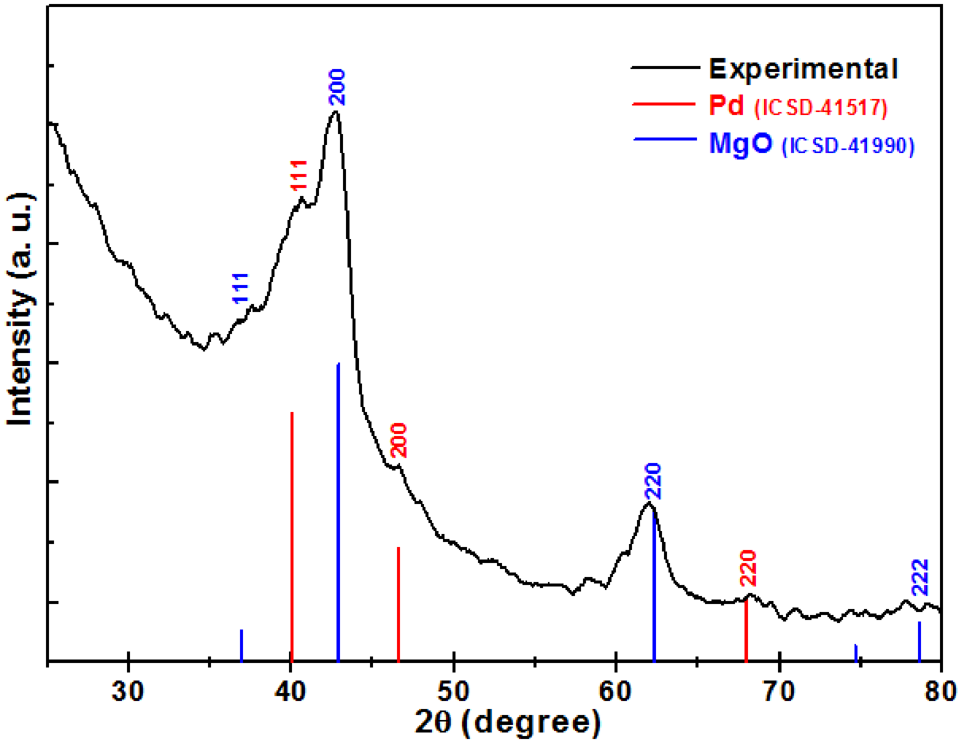

Fig. S2 GIXRD pattern of core-shell Pd@MgO nanoparticles on a silicon substrate at a fixed grazing angle of 0.2°.

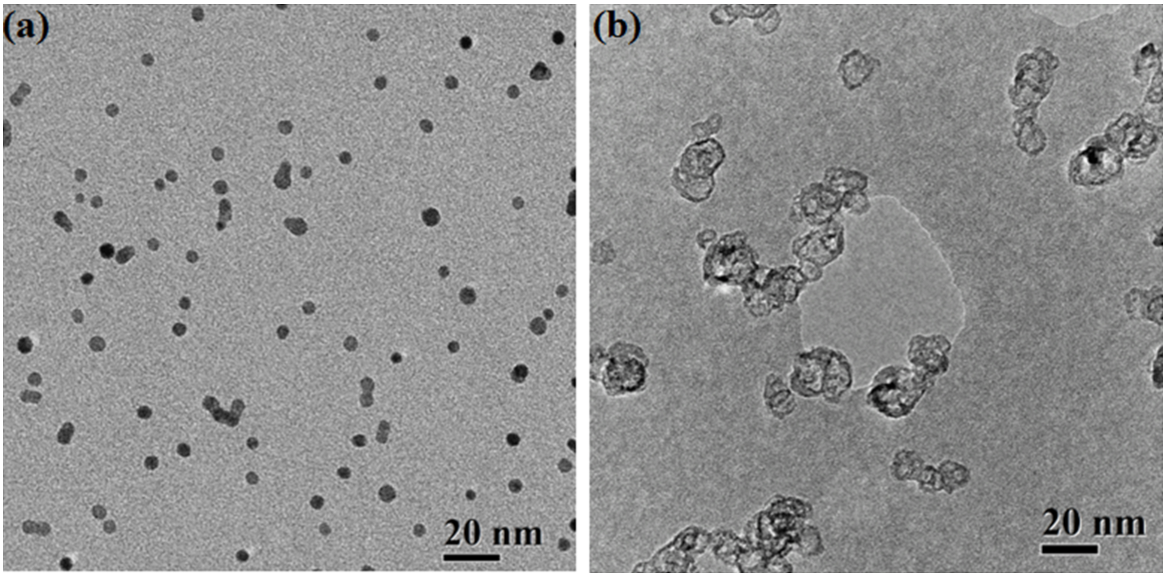

Fig. S3 TEM images of (a) Pd and (b) MgO nanoparticles, deposited separately. It is evident that the MgO structures have formed porous hollow shells (as reported previously).[2]

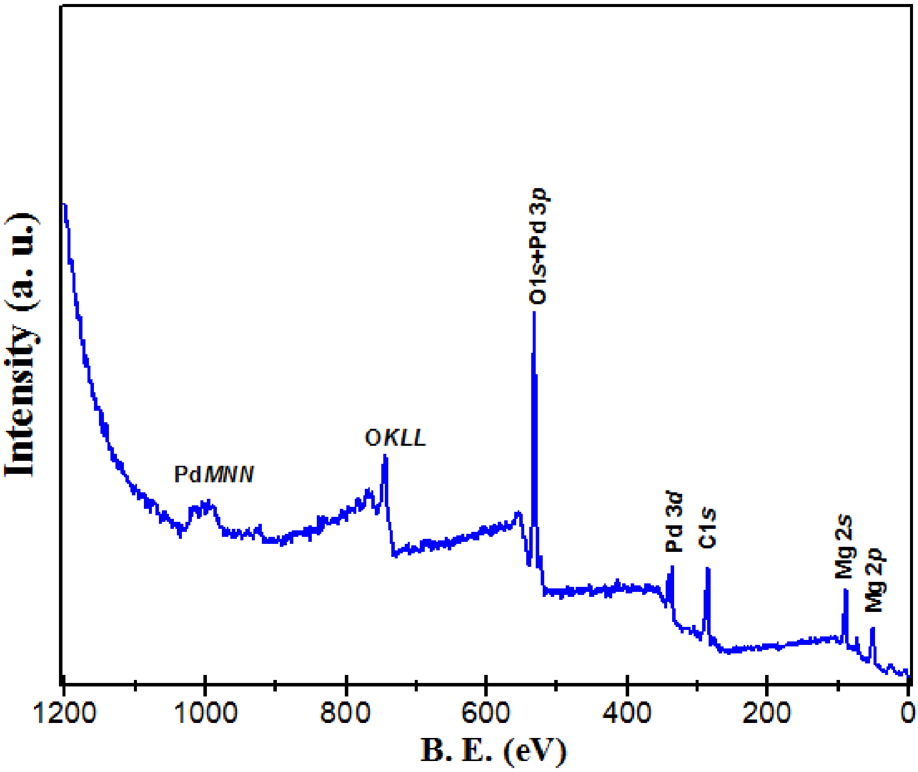

Fig. S4 XPS survey spectrum of core-shell Pd@MgO nanoparticles.

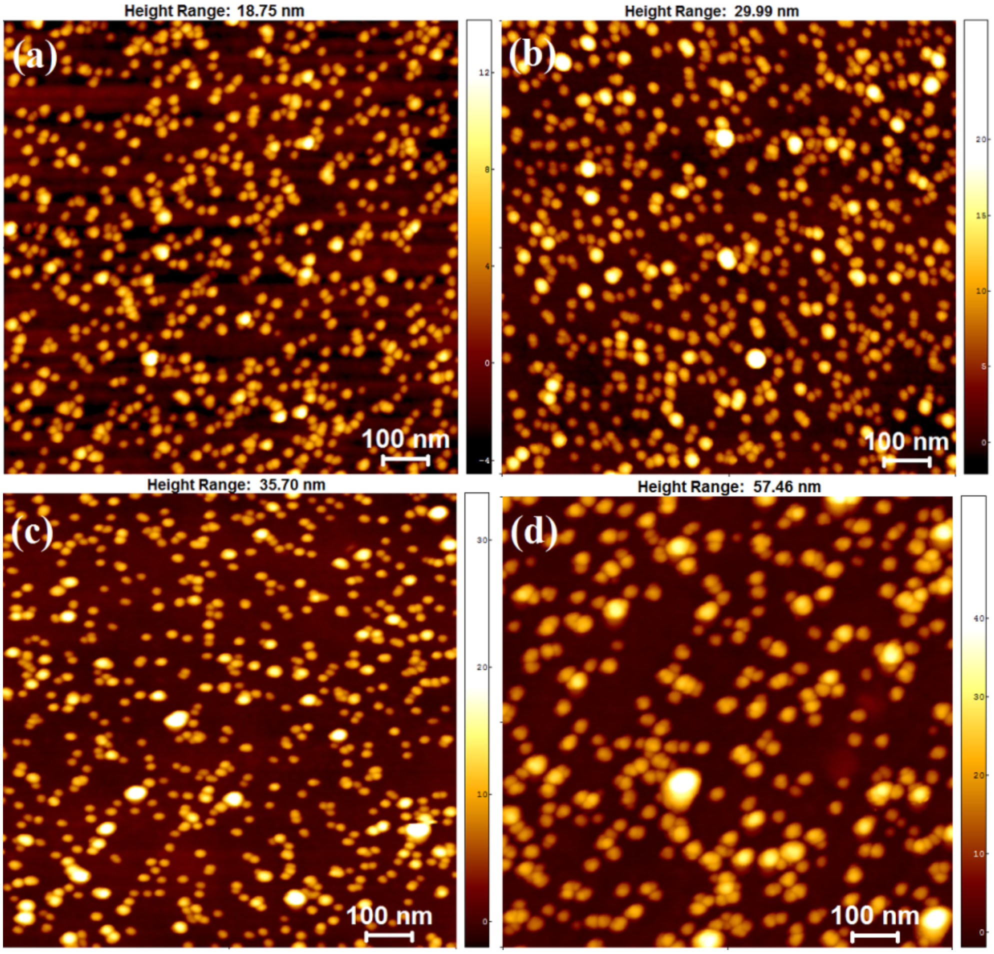

Fig. S5 AFM images of Pd@MgO nanoparticles for different Pd/Mg sputtering power ratios; (a) 0.66, (b) 0.33, (c) 0.14, and (d) 0.11.

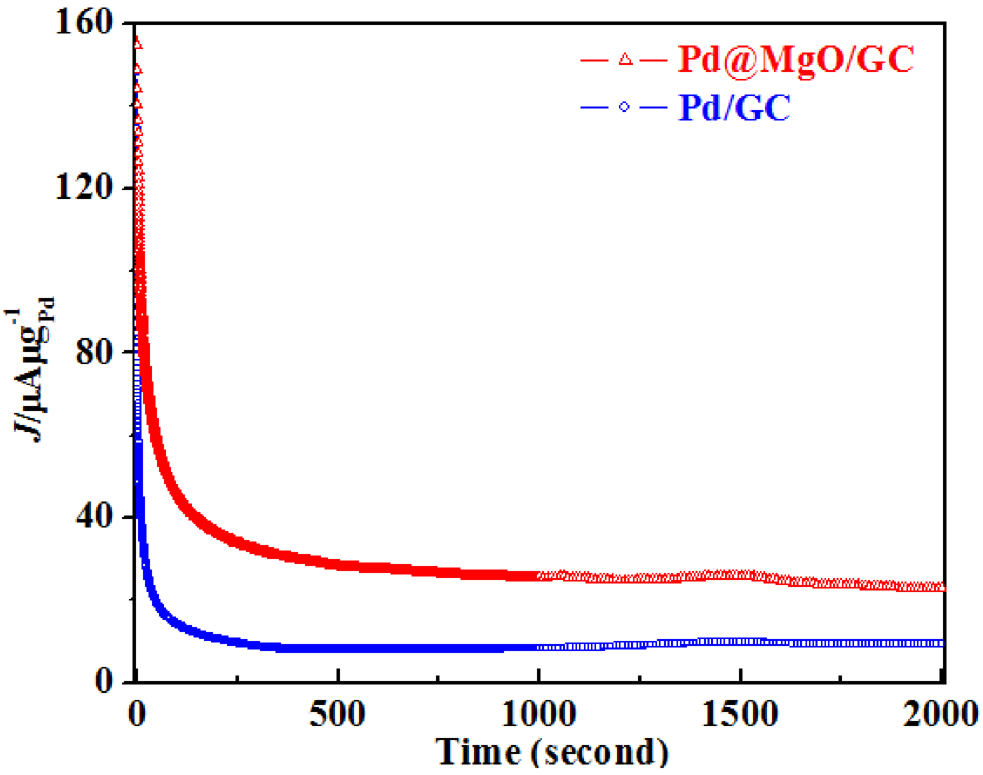

Fig. S6 Current time curves measured by chronoamperometry for Pd/GC and Pd@MgO/GC nanocatalysts at -0.35 V (*vs*. AgCl). in N_2-saturated 1 M KOH containing 0.5 M methanol.

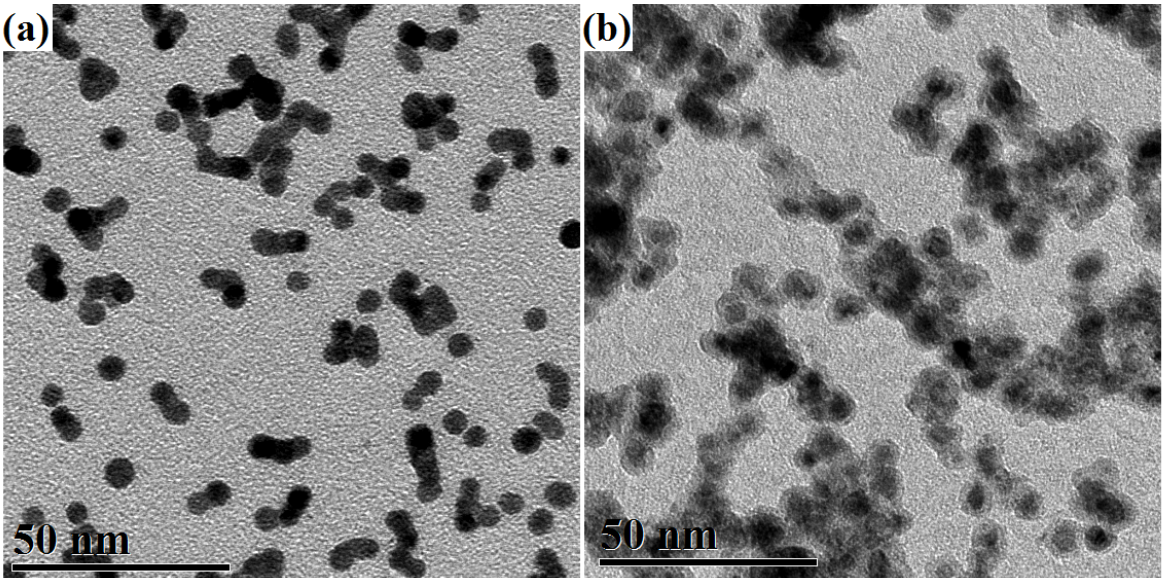

Fig. S7 TEM images of (a) coalesced Pd nanoparticles and (b) Pd@MgO core-shell nanoparticles. These samples were used for the cyclic voltammetry measurements.

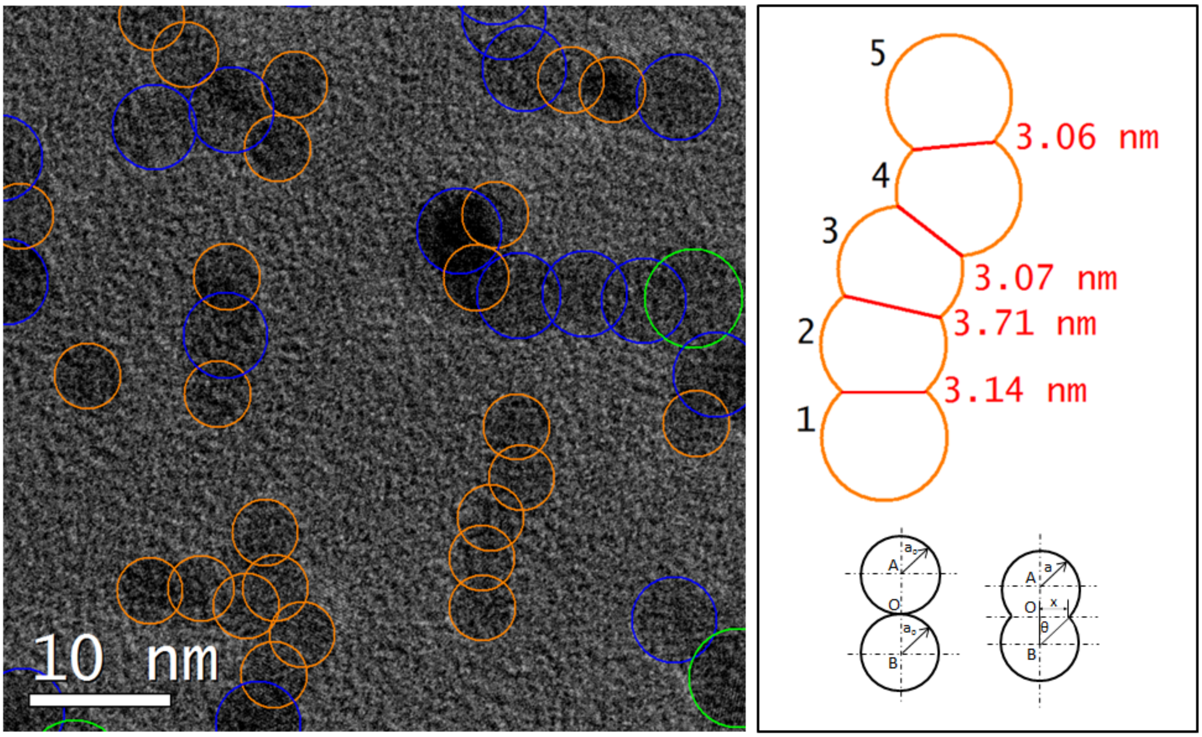

Fig. S8 Surface area loss as a result of nanoparticle coalescence on the substrate. Particles were identified according to the original nanoparticle size (based upon the in-flight mass filter data), identified by the orange circles. Multiples, indicating full coalescence, were also identified (blue and green circles). It is assumed the full coalescence only occurred in-flight, owing to the high temperatures required.[3] Loss of surface area was then determined using the modified Frenkel method for coalesced particles,[4] based upon the degree of interpenetration of the particles.

Supplementary References:

1. P. Stadelmann, “Java Electron Microscopy Simulation (JEMS) software.” *Switzerland: CIME-EPFL, École Polytechnique Fédérale de Lausanne*, 2006.
2. B. J. Kooi, G. Palasantzas andJ. Th. M. De Hosson, *Appl. Phys. Lett.,* 2006, **89**, 161914.
3. P. Grammatikopoulos, C. Cassidy, V. Singh and M. Sowwan, *Sci. Rep.*, 2014, **4**, 5779.
4. O. Pokluda, C. T. Bellehumeur and J. Machopoulos, *AIChE Journal*, 1997, **43**, 3253.